Arch. Metall. Mater. **64** (2019), 4, 1519-1526

DOI: 10.24425/amm.2019.130121

HAROUNE RACHID BEN ZINE*,**, FILIZ CINAR SAHIN***, ZSOLT CZIGÁNY**,
KATALIN BALÁZSI**, CSABA BALÁZSI**#

NOVEL SiC DISPERSION STRENGTHENED AUSTENITIC STEELS PREPARED BY POWDER TECHNOLOGY

In this work, the 316L austenitic steel based milled and sintered composites with 0.33 wt% and 1 wt% SiC ultra-fine particles addition have been prepared. The high efficient attrition milling provided an efficient size reduction of the 316L steel grains and homogeneous distribution of the SiC nanoparticles before sintering process. Spark plasma sintering (SPS) was used for compaction of milled powder mixtures. The effect of SiC addition on the milling efficiency and the structure of the composites have been studied. It was found that the amount of ceramic addition did not influence the efficiency of milling process, powder mixtures with flake like grains have been obtained. On the other hand, the intensive milling assured an optimal coverage of 316L stainless steel grains with submicron sized ceramic particles in both cases. The sintered composites showed high densities with the presence of small amount of closed porosities. Structural, mechanical and tribological examinations of 316L/SiC composites have been performed and presented.

Keywords: SiC dispersion; 316L stainless steel; attrition milling; spark plasma sintering; composite

1. Introduction

The hardness and the wear resistance of the AISI 316L may be improved by dispersion of the SiC in the matrix, the precipitation of the Cr_2C_3 and the Fe_2Si or by the grain refinement [1]. In the case of Spark Plasma Sintering (SPS) the current passes through the lowest resistance areas which can result in heterogeneous sintering of powder samples [2]. A.B. Kale et al. studied the deformation and fracture behaviours of 316L stainless steels fabricated by SPS technique under uniaxial tension and showed the high densities of sintered materials. However, the samples were not sintered homogeneously, therefore, two different fracturing mechanisms have been observed. Firstly, ductile fracture in the fully sintered regions, secondly powder/matrix interface decohesion in the partially sintered regions [3]. The investigations demonstrated that the fracture was started from the partially sintered regions [3]. N. Jahanzeb et al. studied the effect of the microstructure on the hardness heterogenity of disimilar metal joints between 316L stainless steel and SS400 steel. It was found that the strain distribution was locally heterogeneous at higher strains due to the unequal patterns of the γ phase transformation to α' in 316L stainlees steel. The deformation twinning was the dominant mechanism for the 316L during uniaxial tension [4]. The hardness of the SUS316L was improved by the Al additions and the best results have been measured for the Al-50 vol% SUS316L composite. The SUS316L reacted with Al and formed Al_3Fe_4 and $AlFe_3$ during the sintering process. This intermetallic compound improved the corrosion resistance while SUS316L/Al composites exhibit good properties such as high-strength, high-efficiency and light weight [5]. C. Ta et al. investigated 316L/316L-50W/W plate functionally graded materials fabricated by SPS as well. Homogeneous interfaces with less pores have been found after 5 hours milling time. Longer milling time leads to less homogenous joint distribution and it was not optimal for obtaining graded interfaces because more microcracks, holes and intermetallics were created [6]. The volume fraction of tungsten (W) in the 316L matrix was the main factor for improving the hardness of 316L-W composites [7]. 80% compressive strain can improve the 316L hardness with 150% due to the grain refinement and the massive creation of twin boundaries and dislocations [8]. High-Pressure Torsion (HPT) for 10 turns provided a a duplex coarse-grained microstructure of ~42 μm, but the ultrafine-grain size was reduced to ~45 nm during this process. Simultaneously, the χ phase transformed to ε-martensite then to the α'-martensite, this martensitic phase showed exceptional high dislocations density [9]. F. Akhtar et al. improved the sintering densification of the 316L by adding $MoSi_2$. The investigations showed that the Mo and Si segregated at the grain boundaries and the excess formed separate phases. The best mechanical properties were found for samples with 5 wt% MoSi2 [10]. Near full density of 5 wt% Si_3N_4 in 316L has been achieved by liquid phase sintering using high tempera-

* ÓBUDA UNIVERSITY, DOCTORALSCHOOL OF MATERIALS SCIENCE AND TECHNOLOGIES, BÉCSI STR. 96/B, BUDAPEST, HUNGARY
** CENTRE FOR ENERGY RESEARCH, HUNGARIAN ACADEMY OF SCIENCES, KONKOLY-THEGE M. STR. 29-33, BUDAPEST, HUNGARY
*** ISTANBUL TECHNICAL UNIVERSITY, DEPARTMENT OF METALLURGICAL AND MATERIALS ENGINEERING, MASLAK, ISTANBUL 34469, TURKEY
# Corresponding author: balazsi.csaba@energia.mta.hu

ture vacuum furnace. The study showed that the Si_3N_4 was not stable above 2 wt% and it was dissolved in the 316L matrix. The dissociation of much higher amount of Si_3N_4 caused the decreasing of the density due to the diffusion of nitrogen out of the steel matrix [11]. N. Kurgan et al. found that cold pressing under 800 MPa and sintering at 1300°C for 30 minutes in nitrogen atmosphere was more suitable for the 316L powders [12]. The selective laser melting improved the strength of the 316L by the formation of complex microstructure with large angle boundaries, a combination of brittle and ductile fracturing behaviour has been observed. The study proved that the 316L exhibited good mechanical properties at high temperatures [13].

In this paper it was studied the effect of the SiC addition on the properties of the consolidated 316L stainless steels produced by attrition milling and spark plasma sintering.

2. Experimental work

The commercial austenitic 316L stainless steel (Höganäs, 316L) with the composition of 16.8Cr-12Ni-2.5Mo-1.5Mn-0.6Si and ~70 μm average particles size (Fig. 1a) have been milled separately (reference sample) or together with the ultra-fine SiC (H.C. STARCK, UF 25) with average grain size of 200-300 nm (Fig. 1b). The attritor milling (Union Process, type 01-HD/HDDM) has been used for dispersion of the SiC particles in the steel matrix and for a simultaneous size reduction of 316L grains at 600 rpm in ethanol for 5 h. The stainless-steel tank, agitator, and grinding media with 3 mm in diameter have been used for milling. Spark plasma sintering (SPS, Sinter-SPS-7.40MK-VII) has been used for sintering the milled powders at 900°C under 50 MPa mechanical pressure for 5 min in vacuum (6 Pa). Sintered solid disks with ~100 mm diameter and ~9 mm thickness have been obtained. The INSTRON 2500 equipped with special 3 point bending test setup has been used to measure the flexural strength of the samples. The tribological properties of the sintered samples have been determined at room temperature in dry condition using the CSM+ HT Tribometer. Different grinding papers (grade up to 100 μm) have been used for polishing the samples before measuring the tribological properties. 5 N normal load was applied to the counterpart Si_3N_4 ball 5 mm in diameter against the steel sample surface with 1mm shift from the rotation axe of the sample.

The Scanning Electron Microscopy (SEM, Zeiss-SMT LEO 1540 XB) and Transmission Electron Microscopy (TEM, Philips CM-20 with 200 kV acceleration voltage) were used for structural and morphological investigations of base powder, milled, and sintered samples. The elemental compositions of sintered samples were measured by Energy Dispersive Spectroscopy (EDS) installed on SEM LEO microscope. Phase analyses were performed by X-ray diffractometer (XRD, Bruker AXS D8) with CuKα radiation. The hardness of sintered SiC ceramic dispersion strengthened steels (CDS) composites was measured by Vickers method 5 N applied load for 30 s.

3. Results and discussions

The investigation of the milled powders revealed a total morphological transformation. The 316L steel grains in the case of the milled 316L/0.33 wt% SiC powder mixtures have been transformed from globular shape with satellites to considerably larger steel grains with 100-200 μm in diameter and ~1 μm in thickness (Fig. 2a). The presence and the good distribution of the SiC particles on the 316L grains surface and a difference in the size of the SiC particles have been observed by SEM (Fig. 2b). A homogeneous coverage of flat steel grains by ceramic particles can be noticed. In the case of the 316L/1 wt% SiC, a similar morphological transformation has been observed (Fig. 3a). The Fig. 3b shows the presence and the uniform distribution of the SiC particles on the surface of the flat steel grains. SiC particles are covering the steel grains and in the same time show a tendency to agglomerate. This feature can be observed both on the surface of the 316L/1 wt% SiC grains (Fig. 3b) and on the 316L/0.33 wt% SiC grains (Fig. 2b). The structural investigations of the milled powders with composition of 316L/0.33 wt% SiC and 316L/1 wt% SiC by SEM and EDS confirmed the presence of the SiC particles on the surface of the metallic grains (Fig. 4 and 5).

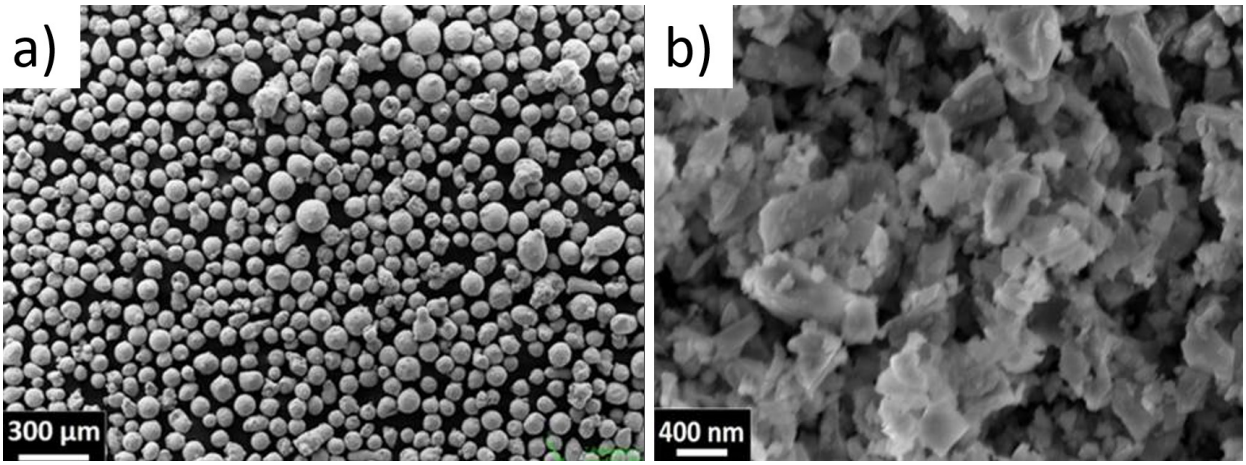

Fig. 1. SEM micrographs of the starting powders a) 316L stainless steel, b) SiC UF 25

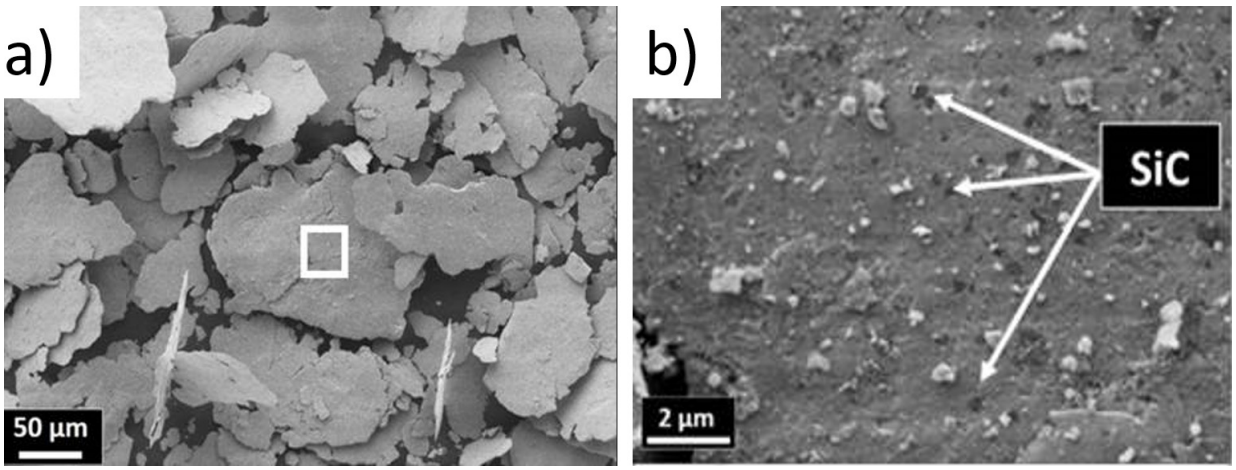

Fig. 2. SEM micrographs of the milled 316L/0.33 wt% SiC. a) milled powders, b) higher magnification of the selected area in Fig. 2a

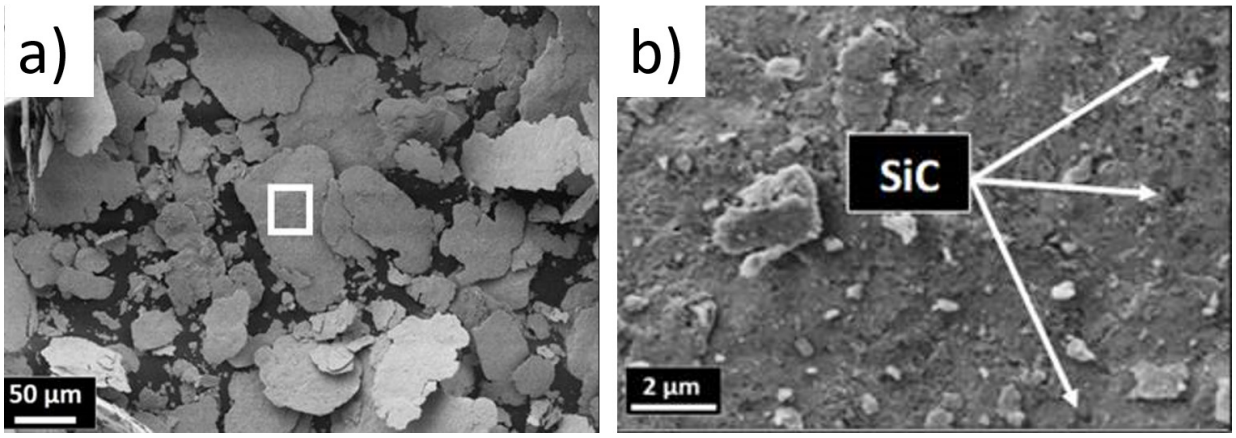

Fig. 3. SEM micrographs of the 316L/1 wt% SiC. a) milled powders, b) higher magnification of the selected zone in Fig. 3a

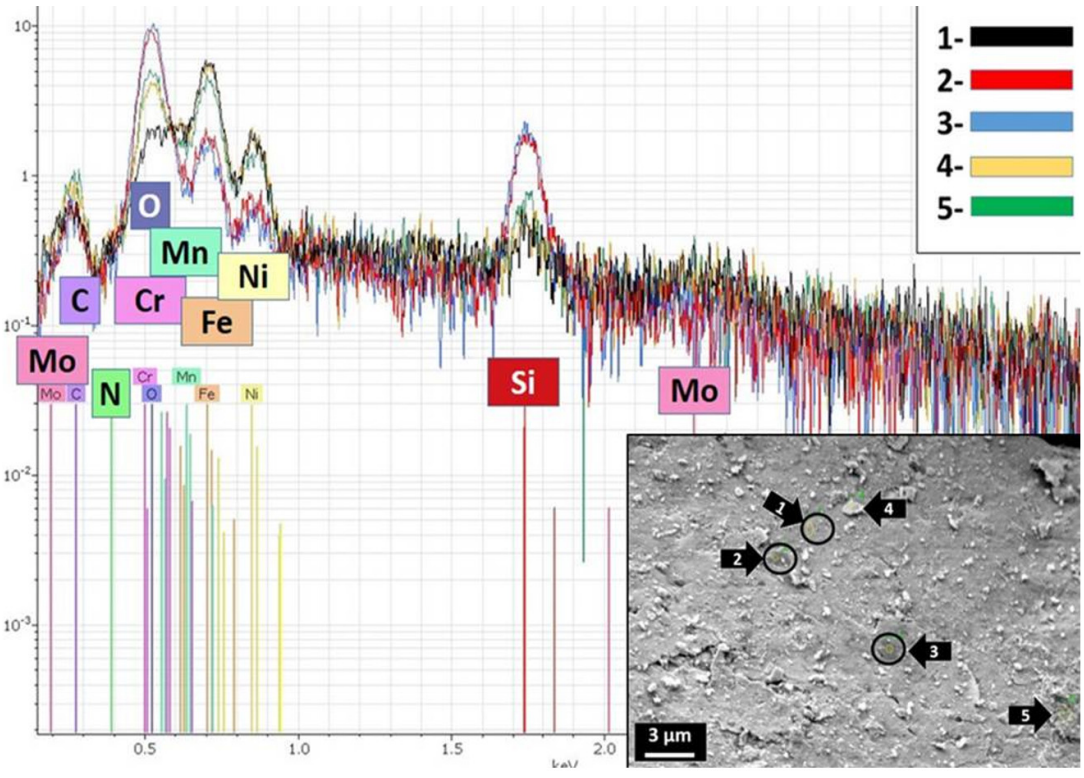

Fig. 4. EDS spectra of the 316L/0.33 wt% SiC and SEM insert showing the EDS spots

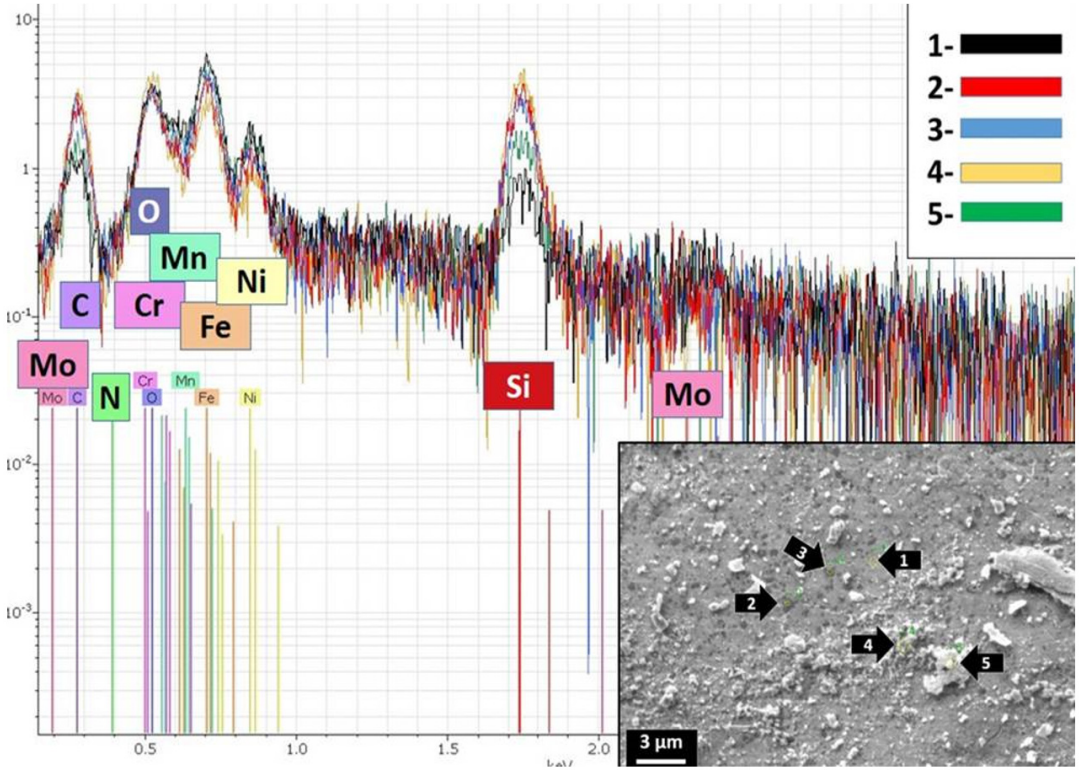

Fig. 5. EDS spectra of the 316L/ 1wt % SiC and SEM insert showing the EDS spots

The relatively lower intensity of peaks related to presence of Fe, Cr and Ni in the selected dark spots shows the good and efficient coverage of the steel grains by the SiC particles.

The phase composition of the milled 316L and 316L/SiC composites have been investigated by XRD. In the case of the milled 316L (reference) the analysis confirmed the austenitic stainless steel γ-Fe_3Ni_2 phase (JPC2:03-065-5131) with main lines 2θ = 43.532°, 50.705°, 74.535° (Fig. 6a). In the case of the 316L/0.33 wt% SiC and 316L/1 wt% SiC composites two phases have been observed, the dominant phase is the same γ-Fe_3Ni_2 austenitic phase in addition to the ferrite α-Fe phase (JCP2: 03-065-4899) with main lines of 2θ = 44.663°, 65.008°, 82.314° (Fig. 6a). The XRD diffractogram of the sintered composites (Fig. 6b) shows that the ferrite α-Fe phase has been transformed to the austenitic γ-Fe_3Ni_2 phase during the sintering process. The investigation of the sintered steel composites surfaces by SEM (Fig. 7) and EDS (Fig. 8 and Fig. 9) shows that dark spots distributed in linear form (white and black parallel lines) consist most probable of SiC particles with oxygen contribution at some extent. The high level of oxygen content in the areas where the SiC particles are distributed indicates the possible oxidation of added SiC particles." Larger silicon oxide

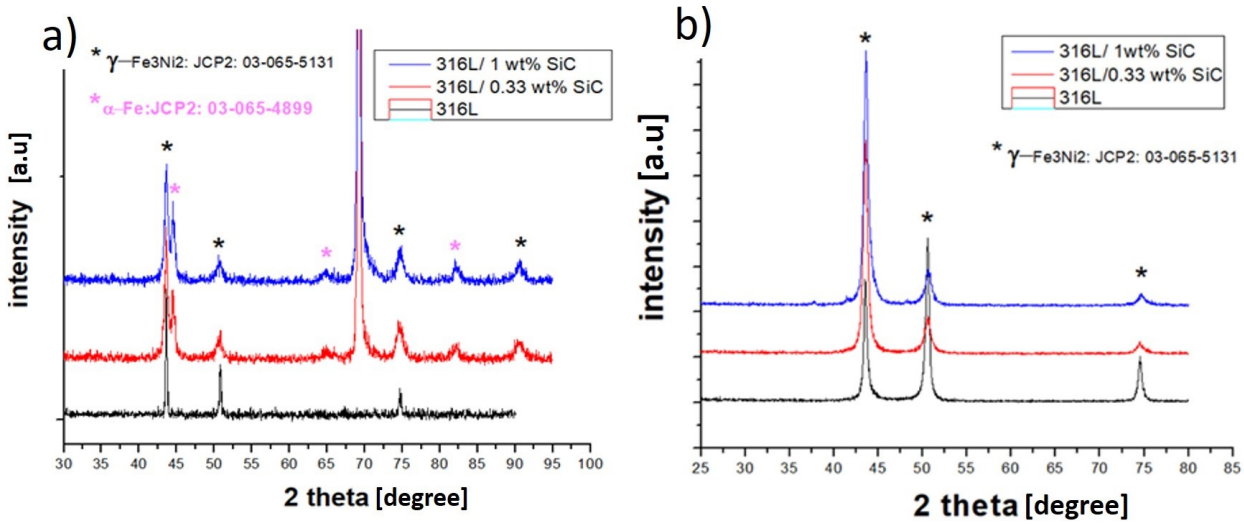

Fig. 6. XRD diffractograms of 316L /SiC a) the milled powder mixtures in comparison with the 316L powder, b) the sintered composites in comparison with the sintered 316L sample

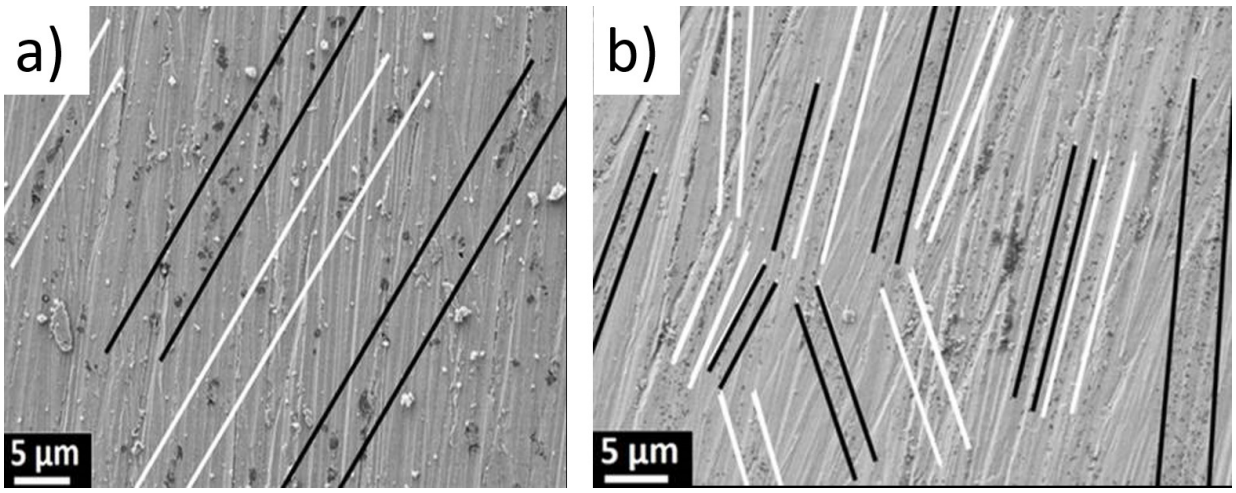

Fig. 7. SEM micrographs of the sintered composites. a) 316L/0.33wt % SiC, b) 316L/ 1wt % SiC

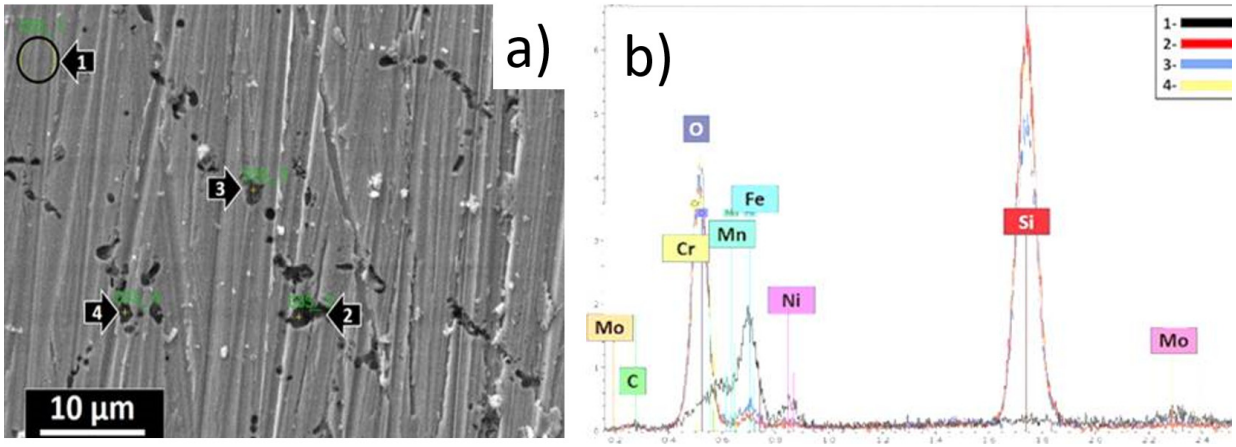

Fig. 8. SEM (a) and EDS (b) investigation of the 316L/0.33wt% SiC

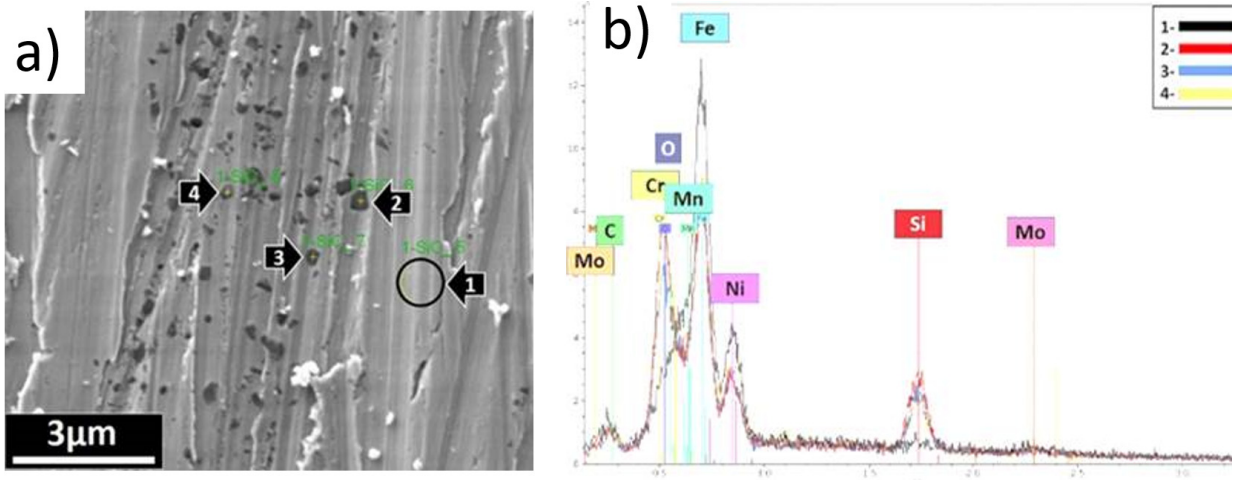

Fig. 9. SEM (a) and EDS (b) investigation of the 316L/1wt% SiC

particles have been observed in the case of 316L/0.33wt% SiC composite as it shown in Fig. 7a and Fig. 8a. An indication for this is the higher peak intensity of the silicon and oxygen in the EDS spectra (Fig. 8b) comparing to the peaks in case of the 316L/1wt% SiC (Fig. 9b).

The density and micro-hardness of the sintered reference sample 316L, 316L/ 0.33wt% SiC and the 316L/ 1wt% SiC composites are shown in Fig. 10. The relative density of 99.17%, 96.66% and 95.2% have been achieved respectively for the 316L reference samples, 316L/ 0.33wt% SiC and the 316L/ 1wt% SiC.

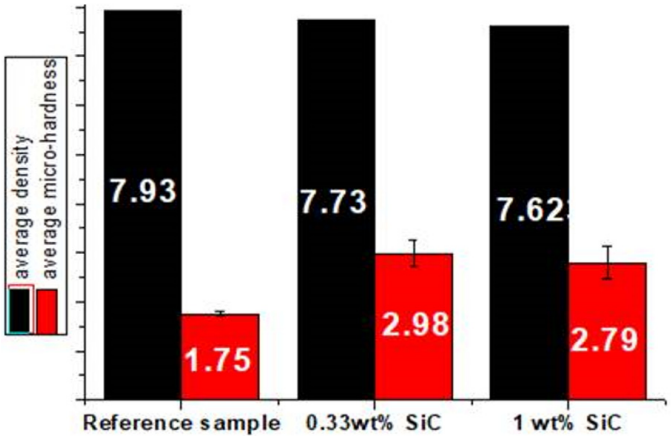

Fig. 10. Comparison of the micro-hardness (GPa) and density (g/cc) of sintered composites

The density of the reference sample is in agreement with literature [3] and it is showing higher values compared to the sintered 316L sintered in special furnace [10-12,14-16] and selective laser melting (SLM) [17-20]. The density decreased with the increase of the SiC amount in the steel matrix. Both composites showed higher micro-hardness values compared to the reference sample (1.75 GPa) and even to those sintered in furnace [10,11,16], SLM [17,18,21] and SPS [5,22]. The lower micro-hardness value in the case of the 316L/ 1 wt% SiC composite (2.78 GPa) compared to the 316L/ 0.33 wt% SiC (2.98 GPa) is due to its lower density.

The Fig. 11a shows the 3 points bending test results of the 316L/ 0.33 wt% SiC composite. The samples were just bended with the presence of very small cracks. As soon the applicable load limit has been achieved the measurement had to be stopped in order to prevent damaging the used equipment (similar to 316L reference sample).

In the case of the 316L/ 1wt% SiC composite (Fig. 11b), the samples were broken and showed an average flexural strength of 1.13±0.1 GPa which is higher than for the 316L SS found in literature [12]. The investigation of the broken surface by SEM (Fig. 12) revealed cracking behaviour/mechanism of the composite which is a mixture of transgranular and intergranular, as

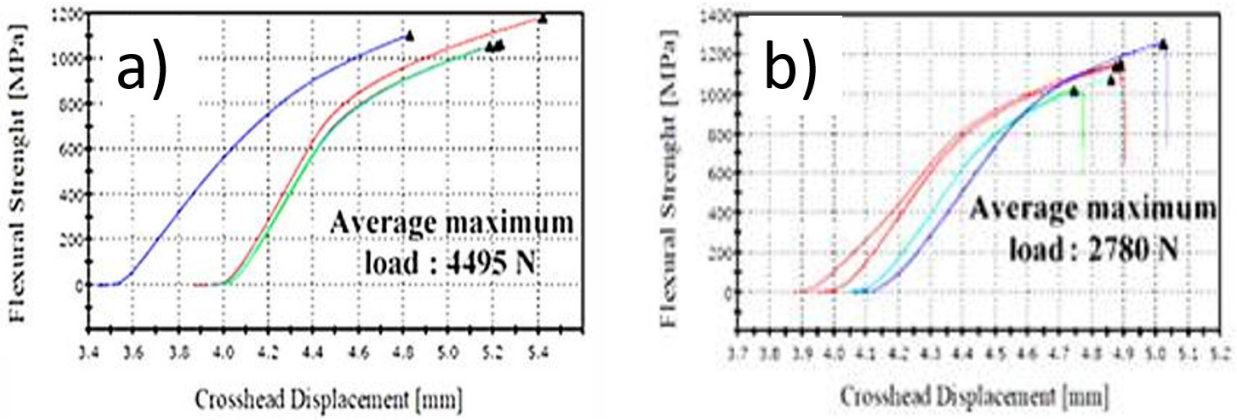

Fig. 11. 3 point bending test results. a) 316L/ 0.33wt% SiC, b) 316L/1wt% SiC

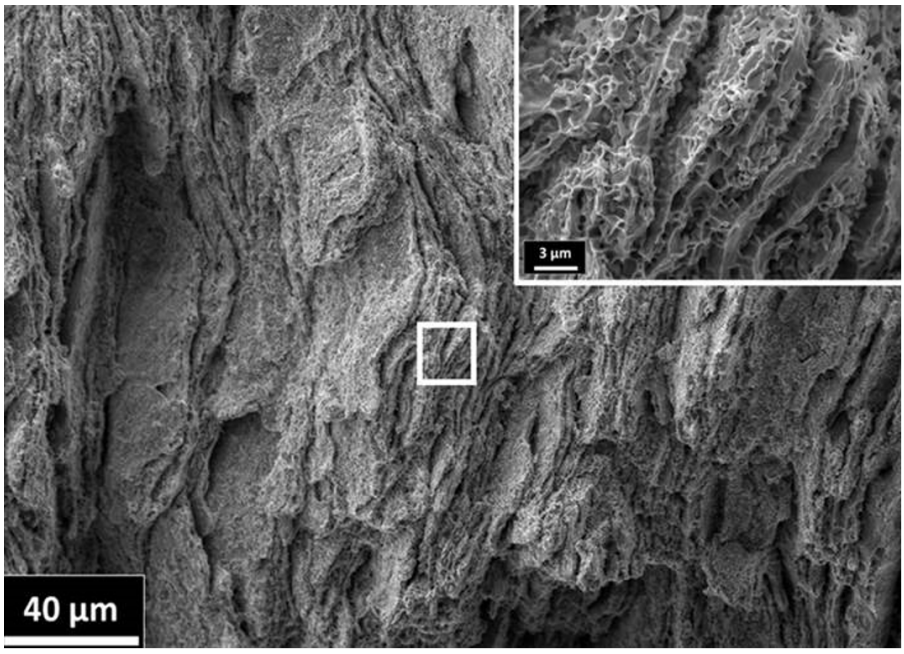

Fig. 12. SEM micrograph of the 316L/1wt% SiC fractured surface

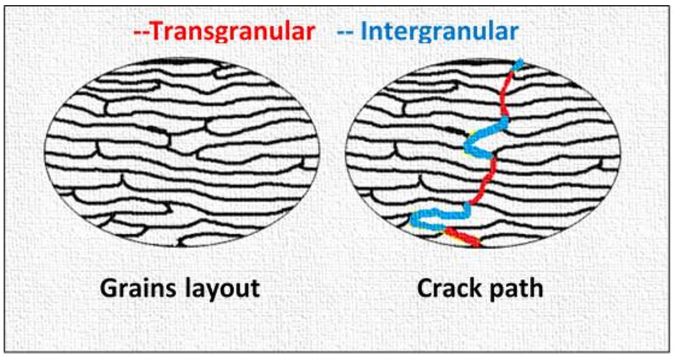

Fig. 13. Schematic representation of the cracking behaviour of the 316L/1wt% SiC

it is illustrated in the Fig. 13. Metallic bridges have been formed between the lamellar steel grains during the sintering process and it is clearly shown in Fig. 12 (insert). Complex grains boundaries have been observed.

Tribological properties of the sintered composites have been studied, the friction coefficients of 0.962, 0.879 and 0.930 have been determined respectively for all of the sintered reference sample 316L, 316L/ 0.33wt% SiC and the 316L/ 1wt% SiC composites. An erosion has been noticed on the tested surface and the Si_3N_4 ball counterpart in all cases. The investigation of the damaged and eroded surface by SEM and EDS showed the formation of tribo-layer on the steel surface as it is shown in Fig. 14. The tribolayers most probably consist of the crytsalline or amorphous main Si_3N_4 originating from the silicon nitride ball. The higher friction coefficient in case of the 316L/ 1wt% SiC (Fig. 14a) composite compared to the 316L/ 0.33wt% SiC (Fig. 14b) composite is due to its lower density and lower hardness. The Fig. 15 shows the TEM image of the sintered 316L/0.33wt% SiC and 316L/ 1wt% SiC composite. The TEM images are showing 50-100 nm white rounded spots that are the ceramic particles embedded into steel micro-grains (Fig. 15a and 15b). In the case of the 316L/ 1wt% SiC composite a better distribution of smaller (50-100 nm) ceramic particles (white rounded particles covering the larger steel grains) have been observed in agreement with EDS and SEM investigations.

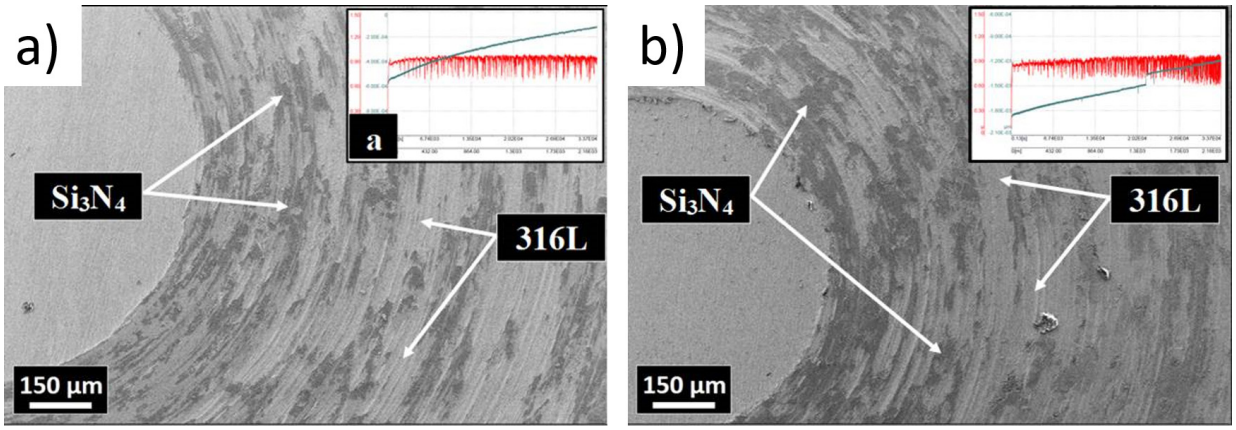

Fig. 14. SEM micrograph of the damaged surface of the 316L/SiC after tribology test and friction coefficient curve (insert). a) 1wt% SiC, b) 0.33 wt% SiC

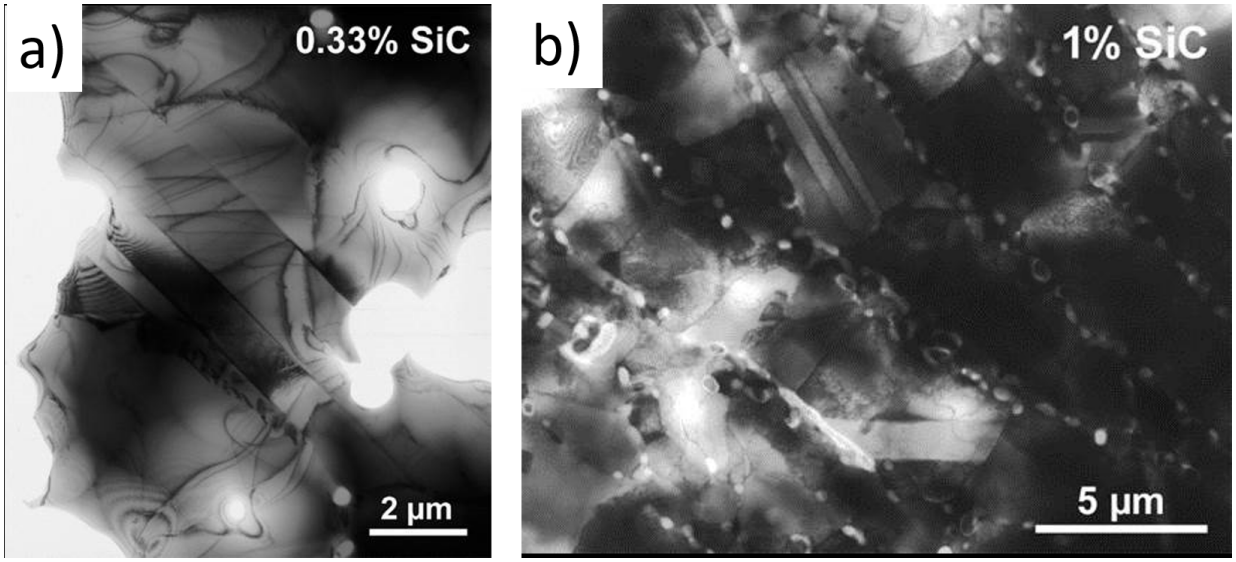

Fig. 15. Bright field TEM images of the sintered 316L/SiC composite. a) 0.33 wt% SiC, b) 1 wt% SiC

4. Conclusions

The preparation of ceramic dispersion strengthened steel with different compositions by attrition milling and spark plasma sintering using commercial 316L and SiC powders was successful. The distribution of the SiC particles was homogenous in both composites. A ferrite phase have been detected in the milled powders due to austenite-martensit transformation or contamination from the milling setup. This ferrite phase has been transformed to the γ-Fe_3Ni_2 during the sintering process. Densification of 99.17%, 96.66% and 95.2 % have been achieved respectively for the reference, 316L/0.33wt% SiC and 316L/1wt% SiC samples. The density decreased with higher amount of SiC addition to steel matrix due to its lower density. The SiC addition improved the hardness of the 316L matrix. The sample 316L/1 wt% SiC shows lower hardness compared to the 316L/0.33 wt% SiC composite due to its lower density. A simultaneous transgranular and intergranular fracture behaviour have been observed after the 3 points bending test of the 316L/1wt% SiC composite where an average bending strength of 1127.4 MPa has been recorded. In the case of the 316L/0.33wt% SiC the samples were just bended due to their higher ductility. Tribological properties of the sintered composites have been studied. It was observed that the addition of the SiC improves the tribological properties of the 316L stainless steel. Friction coefficients of 0.962, 0.879 and 0.930 have been measured, respectively, for all of the sintered reference sample 316L, 316L/ 0.33 wt% SiC and the 316L/1wt% SiC composites. The investigation of the sintered composites by TEM confirmed the distribution of the ceramic particles on the grains boundaries.

Acknowledgement

Mr. Haroune Rachid Ben Zine thanks to Hungaricum Stipendium and MTA EK project "Nanostructural ODS steel development" for support. The authors acknowledge the excellent contribution to Zsolt E. Horváth, and Ákos Horváth to the experimental and evaluation. Thanks are due to Hungarian-Japanese Bilateral project „Development of electromagnetic non-destructive evaluation method for aging degradation of chromium steels at high temperatures".

REFERENCES

[1] Jyotsna Dutta Majumdar et al., Trib. Inter. **42**, 750-753 (2009).
[2] Jinhua Yang et al., Materials and Design **52**, 179-189 (2013).
[3] Amol B. Kale et al., Mat. Sci. & Eng. A **707**, 362-372 (2017).
[4] Nabeel Jahanzeb et al., Mat. Sci. & Eng. A **700**, 338-350 (2017).
[5] Kwangjae Park et al., Mat. Sci. & Eng. A **691**, 8-15 (2017).
[6] Chao Tan et al., Fusion Eng. and Des. **125**, 171-177 (2017).
[7] Chao Tan et al., J. of Nucl. Mat. **469**, 32-38 (2016).
[8] Ankur K. Agrawal, Aparna Singh, Mat. Sci. & Eng. A **687**, 306-312 (2017).
[9] Jenő Gubicza et al., Mat. Sci. & Eng. A **657**, 215-223 (2016).
[10] Farid Akhtar et al., J. of Alloys and Comp. **509**, 8794-8797 (2011).
[11] Akhtar Farid et al., Mat. Sci. and Eng. A **472**, 324-331 (2008).
[12] N. Kurgan, R. Varol, Powder Techn. **201**, 242-247 (2010).
[13] K. Saeidi et al., Mat. and Design **135**, 1-8 (2017).
[14] J. Won Oh et al., Powder Technology **322**, 1-8 (2017).
[15] K. Verhiest et al., J. of Nucl. Mat. **428**, 54-64 (2012).
[16] M. Rafi Raza et al., J. of Mat. Proc. Techn. **212**, 164-170 (2012).
[17] Zhao Shuming et al., Optics and Laser Techn. **103**, 239-250 (2018).
[18] Bandar Al Mangour et al., Mat. and Design **104**, 141-151 (2016).
[19] Bandar Al Mangour et al., Mat. and Design **138**, 119-128 (2018).
[20] Bandar Al Mangour et al., J. of Alloys and Comp. **706**, 409-418 (2017).
[21] Xinwei Li et al., Mat. and Design **145**, 1-10 (2018).
[22] Dandan Guan et al., Vacuum **148**, 319-326 (2018)